Electronic Supplementary Material (ESI) for Energy & Environmental Science.

Supporting Information

Direct tracking the polysulfide shuttling and interfacial evolution in all-solid-state lithium-sulfur batteries: a degradation mechanism study

Yue-Xian Song,[ac] Yang Shi,[ac] Jing Wan,[ac] Shuang-Yan Lang,[ac] Xin-Cheng Hu,[ac] Hui-Juan Yan,[ac] Bing Liu,[bc] Yu-Guo Guo,[ac] Rui Wen,[*ac] Li-Jun Wan[ac]

[a]Key Laboratory of Molecular Nanostructure and Nanotechnology, Beijing National Laboratory for Molecular Science, CAS Research/Education Center for Excellence in Molecular Sciences, Institute of Chemistry, Chinese Academy of Sciences, Beijing 100190, China.

[b]State Key Laboratory of Polymer Physics and Chemistry, Beijing National Laboratory for Molecular Sciences, Institute of Chemistry, Chinese Academy of Sciences, Beijing 100190, China.

[c]University of the Chinese Academy of Sciences, Beijing 100049, China.

[*]**Corresponding Author:** ruiwen@iccas.ac.cn

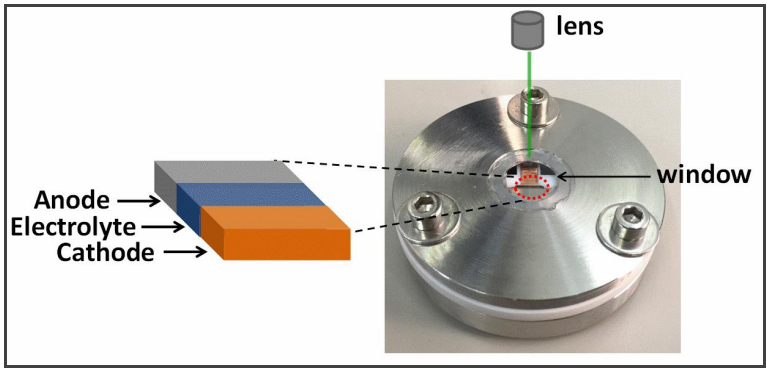

Fig. S1 Schematic of the three-layered sheets (left) and optical image top view (right) of all-solid-state lithium-sulfur cell.

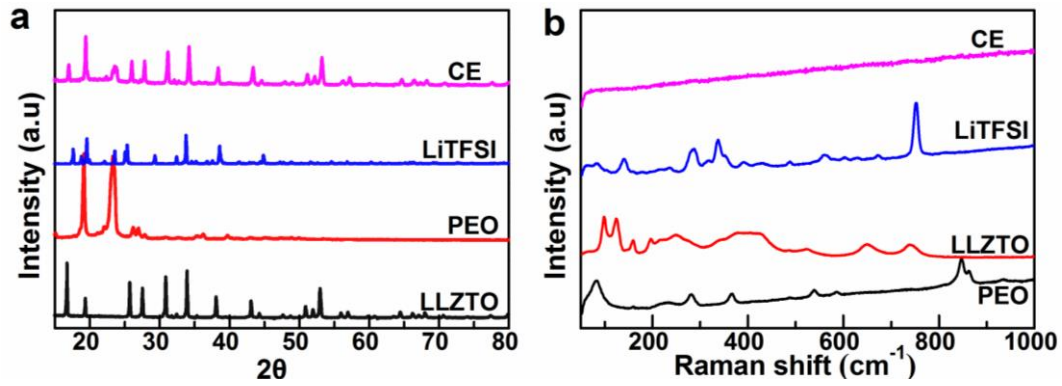

Fig. S2 XRD patterns (a) and Raman spectra (b) of CE membrane, LiTFSI, PEO and LLZTO powders.

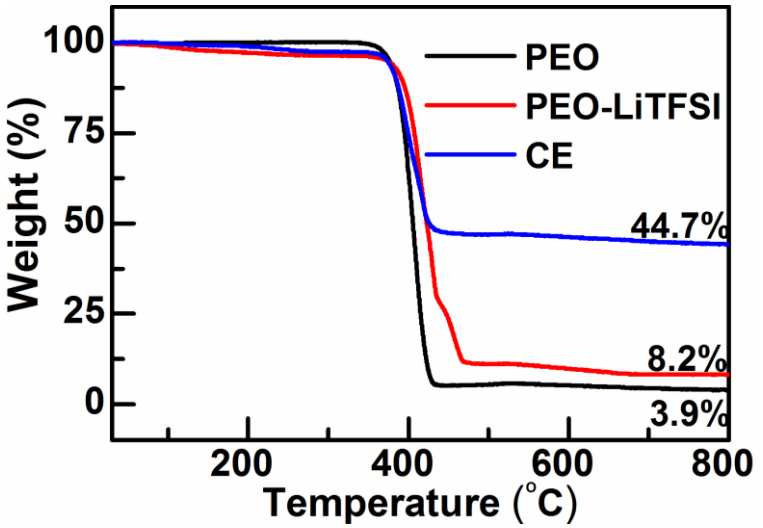

Fig. S3 Thermogravimetric analysis (TGA) curves of the PEO, PEO-LiTFSI and CE membranes.

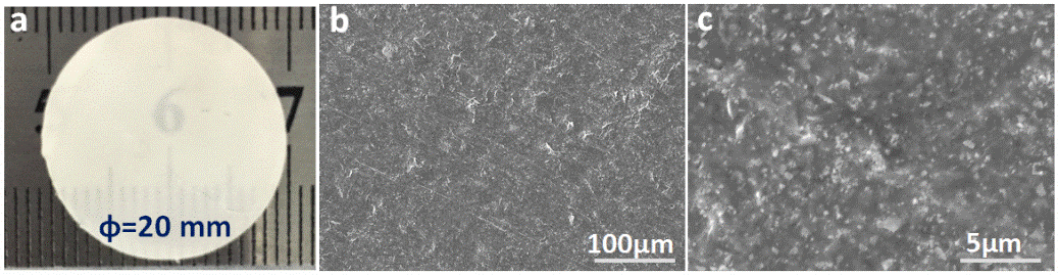

Fig. S4 Photograph (a) and SEM images (b and c) of CE membrane.

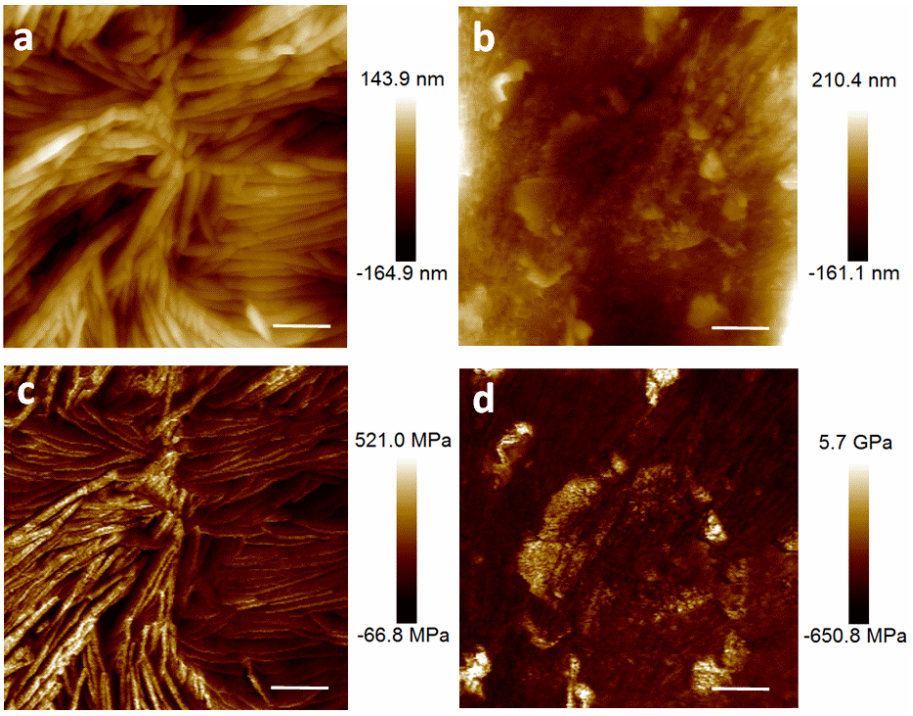

Fig. S5 AFM topography and modulus images of PEO-LiTFSI polymer electrolyte (a and c) and PEO-LiTFSI-LLZTO CE (b and d). The scale bars are 500 nm.

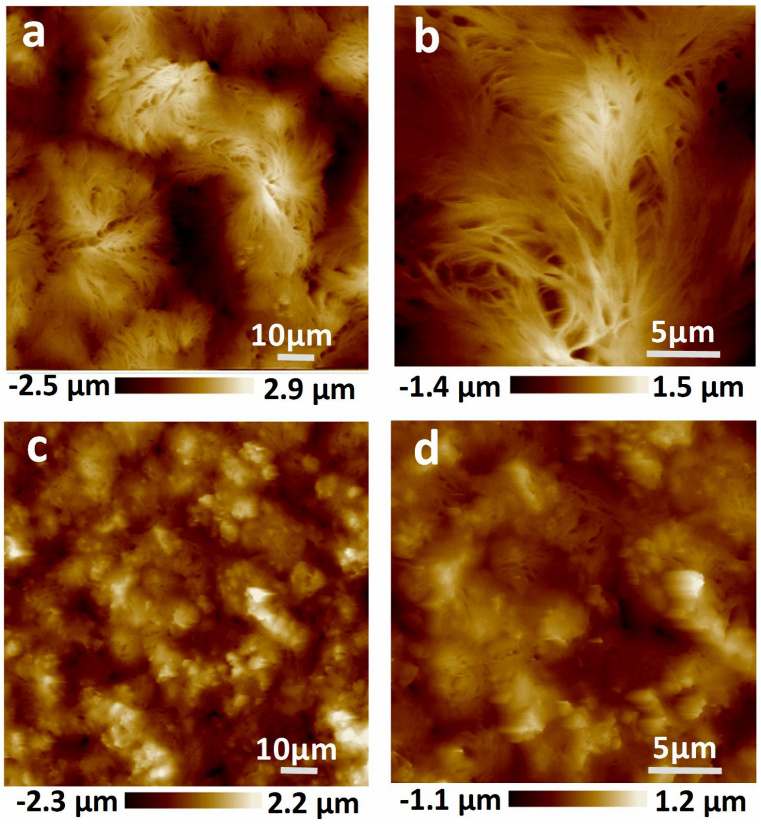

Fig. S6 AFM topography images of PEO-LiTFSI polymer electrolyte (a and b) and PEO-LiTFSI-LLZTO CE (c and d).

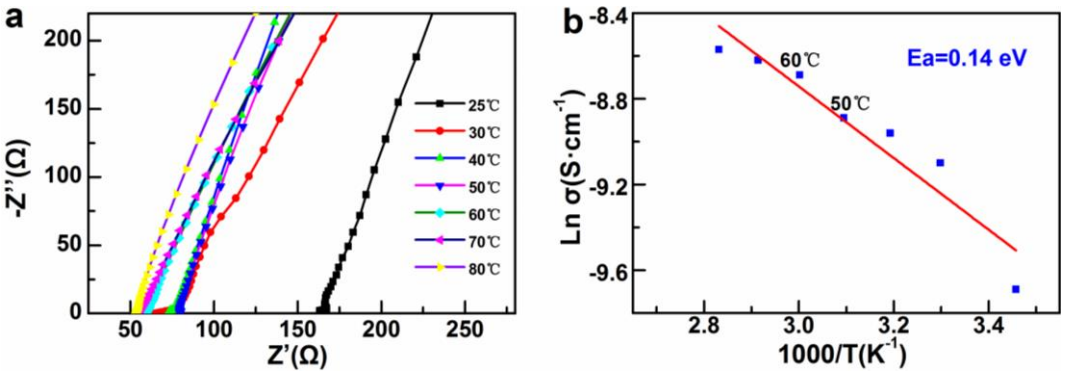

Fig. S7 The impedance spectra (a) and Arrhenius plot (b) of CE from 25 °C to 80 °C.

The ionic conductivity of CEs was calculated based on the following equation:

$$\sigma = \frac{l}{S * R_b} \tag{1}$$

where σ represents the ionic conductivity, R_b is the bulk resistance according to EIS measurement, and l and S are the thickness and area of CE membrane, respectively. Activation energy was calculated from the Arrhenius equation:

$$\sigma = A \exp(\frac{-E_a}{k_b T}) \tag{2}$$

where σ is the ionic conductivity, A is the pre-exponential factor, T is the absolute temperature, K_b is the Boltzmann constant, and E_a is the activation energy.

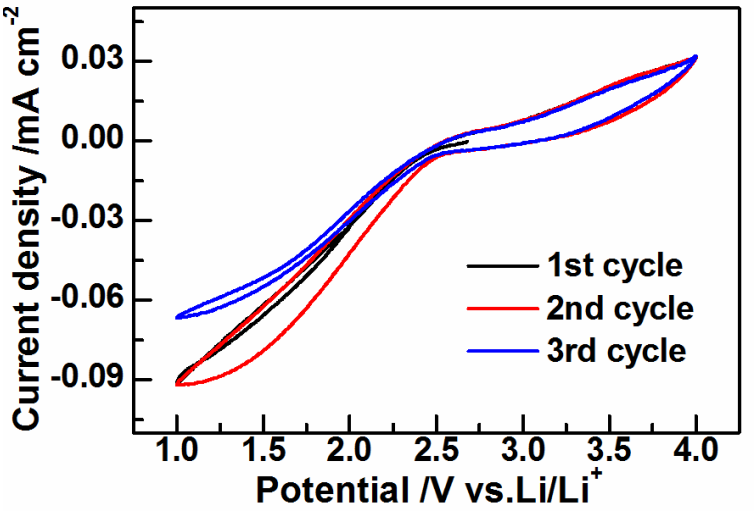

Fig. S8 Representative CV curves acquired for three cycles in the cell without active sulfur of cathode at 65 °C at a sweep rate of 0.5 mV s^{-1}.

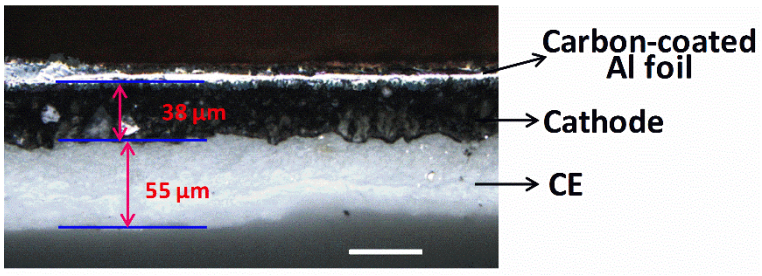

Fig. S9 The cross-section image between active sulfur electrode and solid-state CE of the Li-S batteries before cycling. The scale bar is 50 µm.

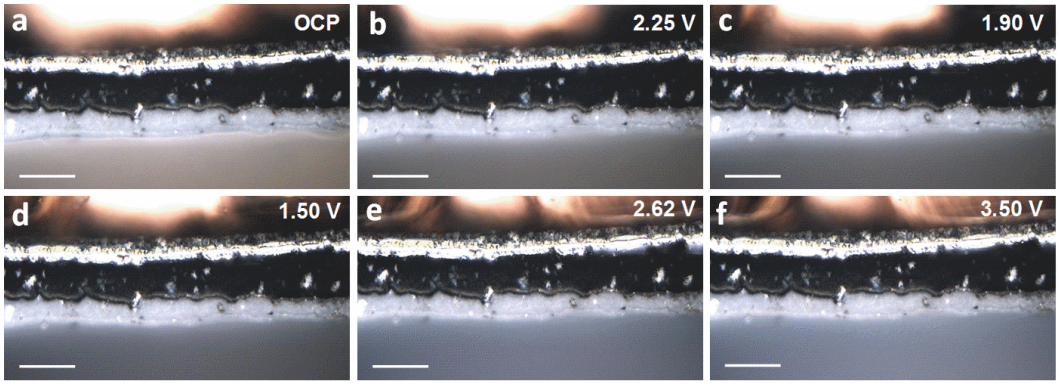

Fig. S10 *In situ* optical imaging acquired at discharging (a-d) and charging (e, f) in the cell without active sulfur of cathode at 65 °C. The scale bars are 100 μm.

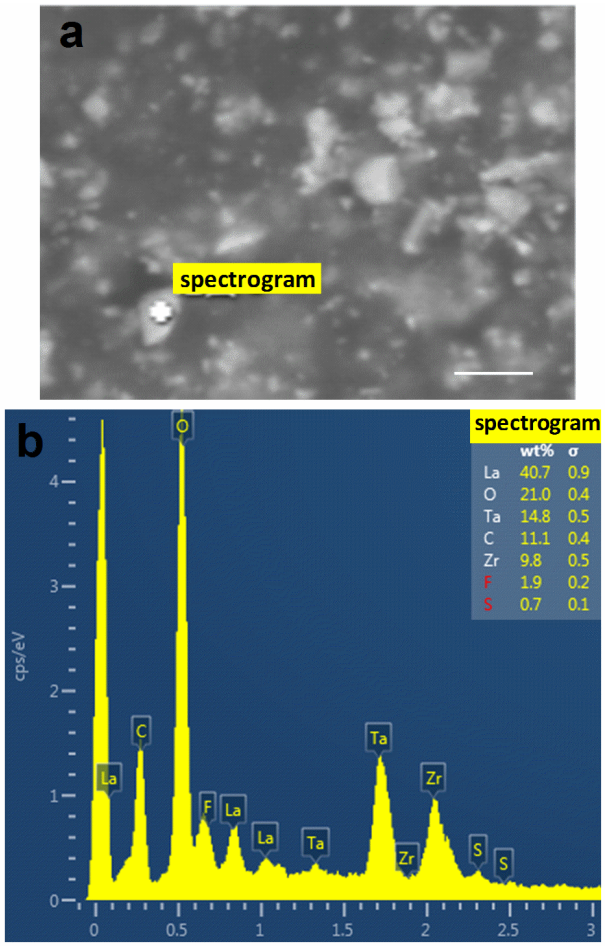

Fig. S11 SEM image (a) and the ratio plot (b) of the initial CE. The scale bar is 500 nm in a.

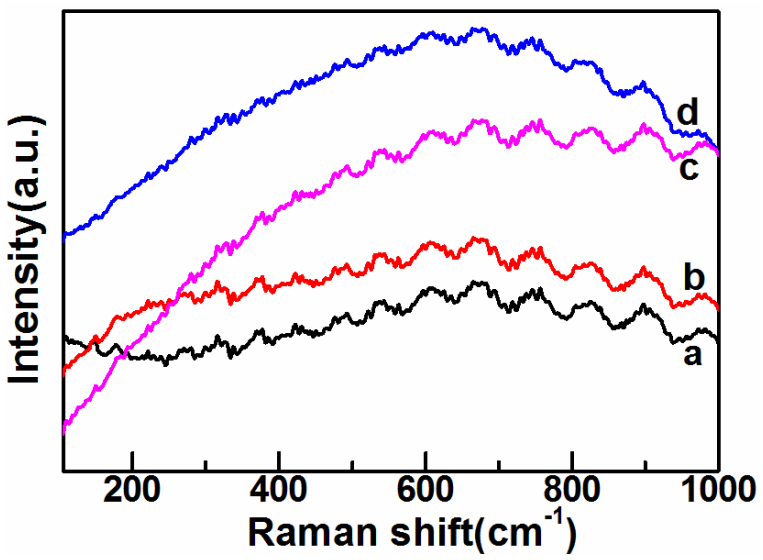

Fig. S12 Raman spectra of CEs obtained in cells without active sulfur of cathode upon discharging to (a) OCP, (b) 2.28 V, (c) 1.79V and charging to (d) 2.62V.

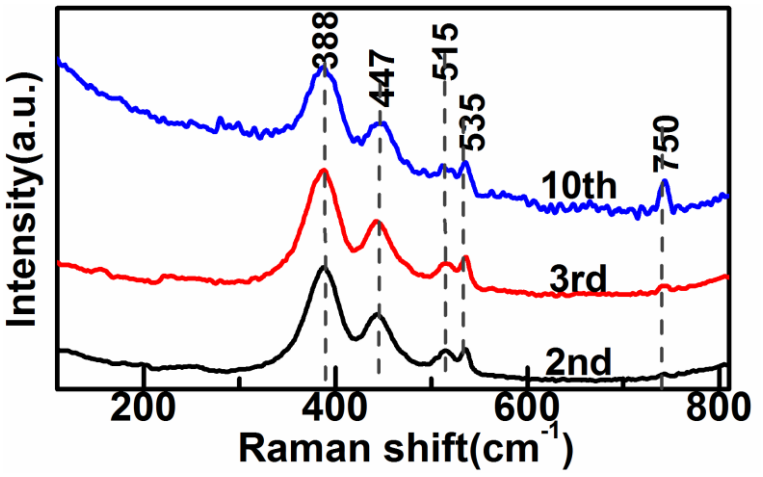

Fig. S13 Raman spectra of CEs acquired after the second, third and tenth discharge-charge cycles.

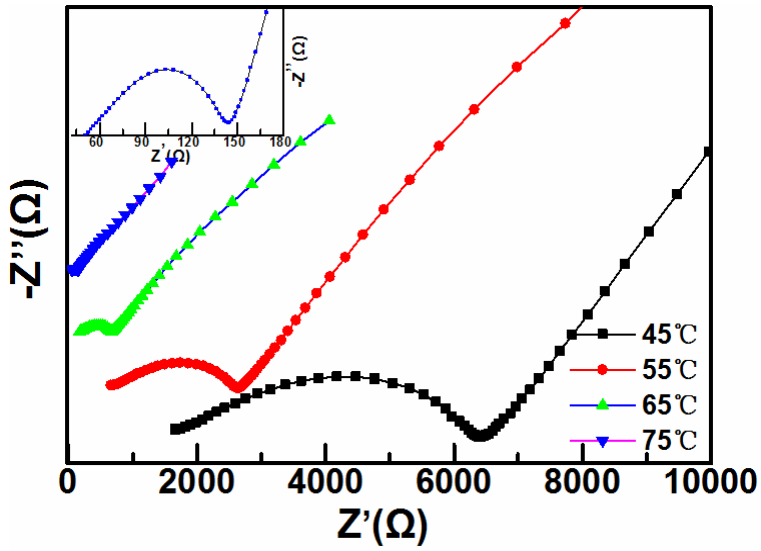

Fig. S14 EIS spectra of all-solid-state lithium-sulfur batteries before cycling at different temperature. Inset is the enlarged curve at 75 °C.

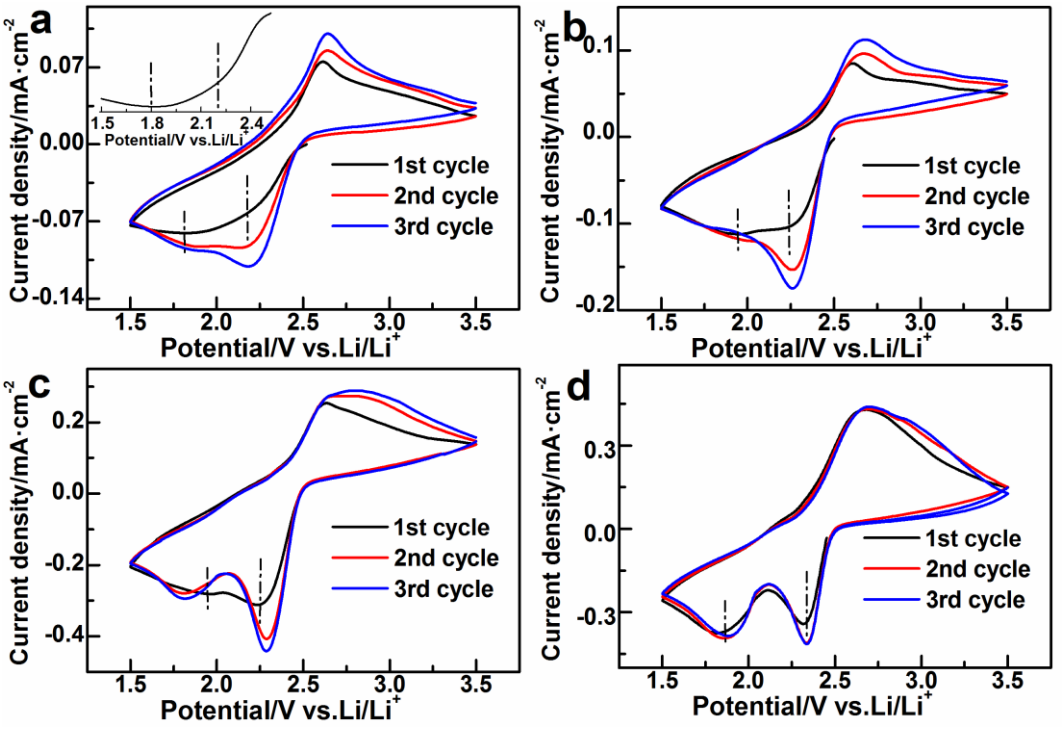

Fig. S15 Cyclic voltammograms of all-solid-state lithium-sulfur batteries at (a) 45 °C, (b) 55 °C, (c) 65 °C and (d) 75 °C for three cycles at a sweep rate of 1 mV s^{-1}. Inset is the enlarged curve near the reductive peaks for the first cycle at 45 °C

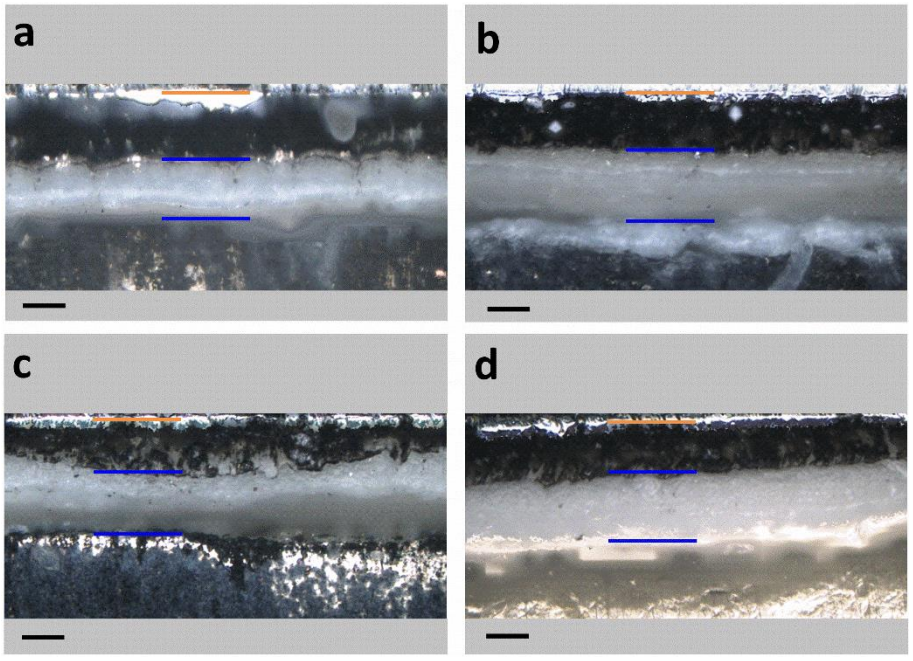

Fig. S16 The optical cross-section images of cells at (a) 45 °C, (b) 55 °C, (c) 65 °C and (d) 75 °C before cycling (OCP). The scale bars are 50 µm.

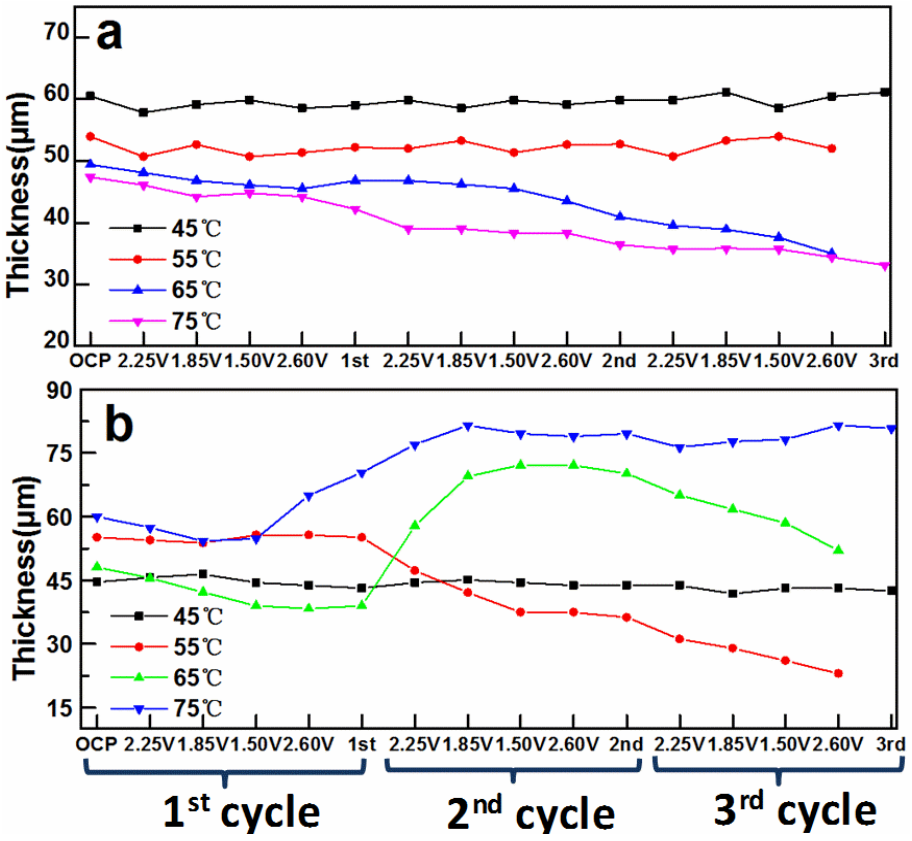

Fig. S17 Variations of the thickness of sulfur cathode (a) and CEs (b) during the cycling processes.

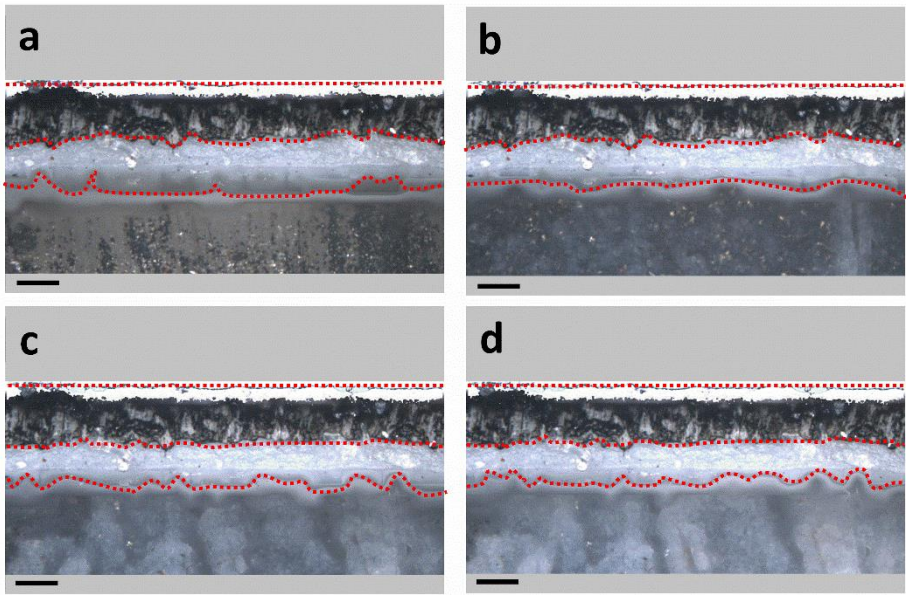

Fig. S18 *In situ* optical imaging of the cell without active sulfur of cathode at 65 °C for (a) OCP, (b) the first cycle, (c) the second cycle and (d) the third cycle. The scale bars are 50 μm. The real time OM imaging was captured along the CV measurement in Fig.S8.

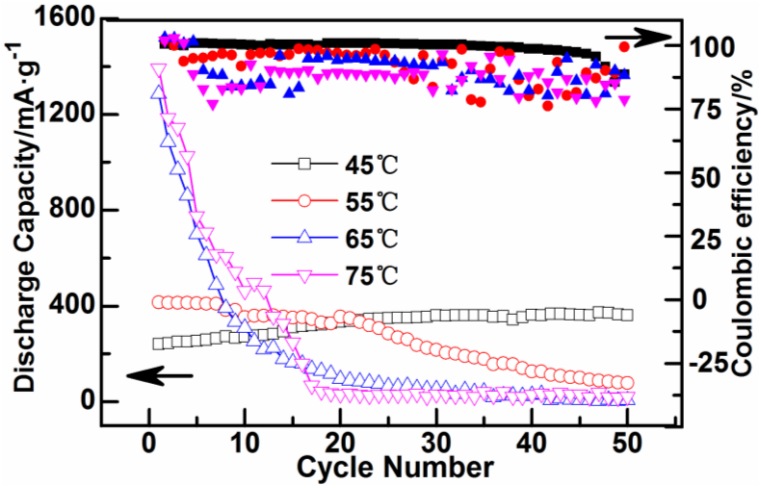

Fig. S19 Discharge capacity and Coulombic efficiency of all-solid-state lithium-sulfur cells at 0.05 mA cm^{-2} at different temperature.

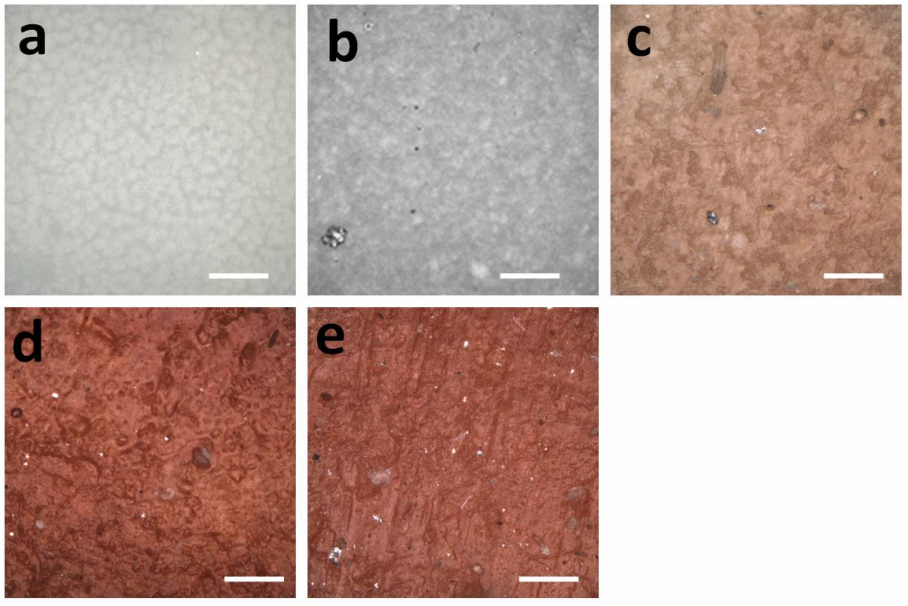

Fig. S20 The optical images of CEs for (a) pristine and after three cycles at (b) 45 °C, (c) 55 °C, (d) 65 °C and (e) 75 °C. The scale bars are 50 μm.

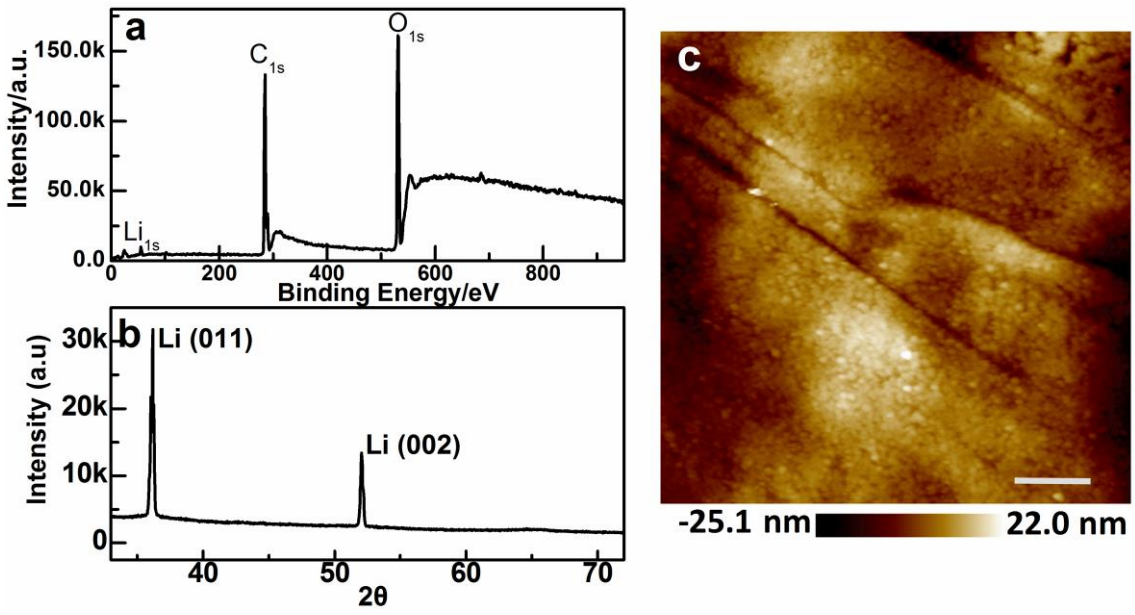

Fig. S21 XPS survey spectrum (a), XRD pattern (b) and AFM topography image (c) of the pristine lithium electrode (uncycled). The scale bar is 500 nm in c.

As shown in Fig.S21, the XPS survey spectrum displays the corresponding peaks of C_{1s}, O_{1s} and Li_{1s}, and XRD pattern indicates that the uncycled lithium anode presents two peaks at 2ϑ= 36° and 52°, which is assigned to the Li (011) and Li (002) planes, respectively.[1] The AFM topography image shows that the compact and flat morphology is visible for uncycled lithium electrode.

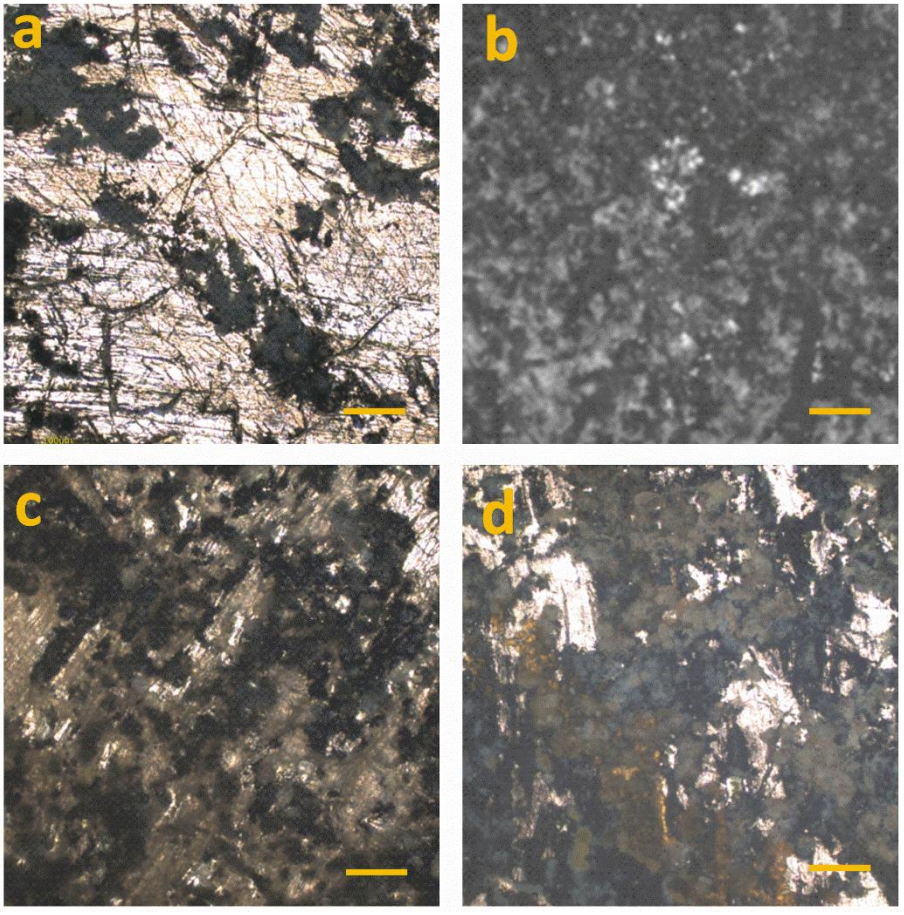

Fig. S22 The optical images of lithium electrode obtained after three cycles at (a) 45 °C, (b) 55 °C, (c) 65 °C and (d) 75 °C. The scale bars are 100 µm.

Table S1. Comparison of the ionic conductivity of PEO-based electrolytes and cycling performance for all-solid-state lithium-sulfur batteries reported from recent literatures.

Electrolyte	Ionic conductivity (S cm^{-1})	Sulfur cathode	The initial discharge capacity (mAh g_{sulfur}^{-1})	Cycle life	Reference
PEO/$Li(CF_3SO_2)_2N$+ SiO_2	ca. 10^{-4} (70°C)	S/mesoporous carbon	1265.5 (@0.1mA cm^{-2})	25	[2]
PEO/$Li(CF_3SO_2)_2N$+ γ-$LiAlO_2$	ca.10^{-4} (65°C)	S/PEO	609 (@0.1mA cm^{-2})	50	[3]
PEO/$Li(CF_3SO_2)_2N$+ MOF(MIL-53(Al))	4.5×10^{-4} (65°C)	S/macrostructural carbon	1457 (@0.5C)	50	[4]
PEO/$Li(CF_3SO_2)_2N$+ MMT	3.22×10^{-4} (60°C)	S@PAN@$Mg_{0.6}Ni_{0.4}O$/AB	998 (@0.1C)	100	[5]
PEO/$Li(CF_3SO_2)_2N$+ LiN_3	3.16×10^{-4} (70°C)	S/Ketien black	1050 (@0.1C)	30	[6]

Video S1. Direct observation of the polysulfide shuttling at the cathode/electrolyte interface in CE-based ASSLS batteries.

Video S2. Direct observation of the structural evolution processes in CE-based ASSLS batteries at 45 °C

Video S3. Direct observation of the structural evolution processes in CE-based ASSLS batteries at 55 °C

Video S4. Direct observation of the structural evolution processes in CE-based ASSLS batteries at 65 °C

Video S5. Direct observation of the structural evolution processes in CE-based ASSLS batteries at 75 °C

References:

1. C. Zu and A. Manthiram, *J. Phys. Chem. Lett.*, 2014, **5**, 2522-2527.
2. X. Liang, Z. Wen, Y. Liu, H. Zhang, L. Huang and J. Jin, *J. Power Sources*, 2011, **196**, 3655-3658.
3. X. Zhu, Z. Wen, Z. Gu and Z. Lin, *J. Power Sources*, 2005, **139**, 269-273.
4. Y. Zhu, J. Li and J. Liu, *J. Power Sources*, 2017, **351**, 17-25.
5. Y. Zhang, Y. Zhao, D. Gosselink and P. Chen, *Ionics*, 2015, **21**, 381-385.
6. G. G. Eshetu, X. Judez, C. Li, O. Bondarchuk, L. M. Rodriguez Martinez, H. Zhang and M. Armand, *Angew. Chem. Int. Ed.*, 2017, **56**, 15368-15372.